BioNanoSci. (2015) 5:189–195
DOI 10.1007/s12668-015-0179-4

Memristive Biosensors for PSA-IgM Detection

I. Tzouvadaki[1] · C. Parrozzani[2] · A. Gallotta[2] · G. De Micheli[1] · S. Carrara[1]

Published online: 28 August 2015

Abstract Prostate cancer is the most common cancer among men except for skin cancer, and the detection at early stages is crucial. In the present work, nanofabricated memristive biosensors are subjected to surface bio-modification targeting at prostate-specific antigen (PSA) IgM detection. The electrical response of the nanofabricated devices examined before and after the bio-modification achieves a label-free detection for three biomarker concentrations. The presence of biomolecules linked to the surface of the nanostructures is detected by a voltage gap appearing in the memristive electrical characteristics. Enzyme-linked immunosorbent assay methodology is further applied to verify the efficiency of the application of diverse biomarker concentrations on the surface. Scanning electron microscopy shows details on the morphology of the nanofabricated structures before and after the bio-modification, and confocal microscopy is implemented to obtain a 3D fluorescent signal distribution of the biomolecules. The system shows the potential for applications in molecular diagnostics and for implementation targeting at the early detection of the prostate cancer disease.

Keywords Silicon nanowire arrays · Memristive behavior · Biosensor · ELISA · PSA-IgM

The present work was financially supported by the project PROSENSE receiving funding from the European Union Horizon 2020 research and innovation program under the grant agreement no 317420

✉ I. Tzouvadaki
ioulia.tzouvadaki@epfl.ch

[1] Integrated System Laboratory, EPFL, Lausanne, Switzerland

[2] Xeptagen Spa, Via delle Industrie, 9, Building Auriga, Venice, Italy

1 Introduction

Immune complexes (ICs) suggest serologic biomarkers which can increase the sensitivity for diagnosing of carcinomas significantly. Main cancer biomarkers circulating in the bloodstream are indicated to associate with immunoglobulin M (IgM) and form stable complexes with diagnostic potential comparable to or greater than that of the corresponding free biomarker. IgM is considered the main component of innate immunity with the binding capacity of a wide range of tumor antigen [1]. Natural IgM plays an important role in the first line of defense against infectious agents, in the regulation of proliferation of immune cells, and in the immunosurveillance against transformed malignant cells [2]. Examples demonstrating the occurrence of cancer biomarkers associated with IgM are reported for different cancer types. Squamous cell carcinoma antigen (SCCA), α-fetoprotein (AFP), and carcinoembryonic antigen (CEA) can be detected complexed to IgM in the serum of patients with cancer. More specifically, when detected as IgM complexes, both AFP—the conventional serological marker for the detection of HCC—and SCCA enable the diagnosis of liver cancer [3–6]. Further evidence of the diagnostic relevance of IgM immune complexes in cancer is also provided by CEA, the serological standard for the diagnosis of colorectal cancer (CRC). The assessment of CEA-IgM levels in CRC patients allows the identification of a much higher number of patients compared to free CEA, and the sensitivity is increased without compromising assay specificity for the co-determination of both biomarkers [7]. For the occurrence of PSA-IgM immune complexes in the serum of patients with prostate cancer, an enzyme-linked immunosorbent assay (ELISA) is usually applied to evaluate the presence of PSA-IgM immune complexes in sera of patients and the efficiency of PSA-IgM detection for prostate cancer diagnosis [8, 9]. Enhancement of diagnostic indexes of PSA-IgM for

cancer diagnosis is observed as PSA-IgM assay improves sensitivity and specificity indexes with respect to prostate-specific antigen (PSA) test. The gain in cancer detection achieved by using this combination may serve as a complementary serological marker of prostate cancer. However, new technologies are now required, especially toward the possibility to detect early traces of cancer markers.

In 2008, Strukov et al. [10] introduced the first physical implementation of a memristor [11] consisting of a two-layer thin film of TiO_2, with one of them doped with oxygen vacancies, sandwiched between platinum contacts. This model demonstrates that memristance may arise naturally in nanoscale systems in which solid-state electronic and ionic transports are coupled under an external bias voltage. The pronounced hysteresis appearing in the electrical characteristics is a unique and important signature of memory devices [12] and has been attributed to a wide range of phenomena, including molecular redox events and metal filament formation and destruction. Memristive devices present a rapidly increasing interest in recent years thanks to the different application they may be used for. Indicatively, memristive systems enable new possibilities for computation and non-volatile memory storage as, for example, the construction of memristor-based digital logic circuits [13], applications regarding artificial synapses [14–16], resistive RAM (ReRAM) memories [17], and generic memristive structure (GMS) for 3D FPGA applications have been proposed [18]. Memristive silicon nanowire devices functionalized with antibody films are recently introduced as memristive biosensors for biosensing purposes [19, 20]. Thanks to the high surface-to-volume ratio that the nanowire structures present, their electrical properties are strongly influenced by minor perturbations [21, 22]. Furthermore, the nanowire structures exhibit tunable electron transport properties, and the charge accumulation or depletion takes place in the bulk of the structure. Consequently, these nanostructures can potentially enable the label-free sensing via direct electrical readout when the nanostructures are used as semiconducting channels of field-effect transistors [23], for example, for cancer markers [24] or DNA [25] detection. In the case of the memristive biosensors [19, 20], the hysteresis loop of the current-to-voltage characteristics of the memristive devices is affected by the presence of biomolecules introducing a voltage difference between the forward and backward zero-crossing points of the current-to-voltage characteristics, the so-called voltage gap.

In the present work, memristive biosensors are fabricated and applied for the detection of PSA-IgM markers. The results obtained via the electrical characteristics methodology are correlated and verified with enzyme-linked immunosorbent assay measurements. Scanning electron microscopy and confocal microscopy throw details on the morphology of the fabricated structures and the distribution of the biomolecules, respectively.

2 Materials and Methods

2.1 Fabrication of Memristive Silicon Nanowires

2.1.1 Memristive Devices

Memristive silicon nanowire devices are fabricated using commercially available (100) oriented silicon on insulator (SOI) substrate with low boron concentration. Electron beam lithography is applied to the substrate after coating with Poly(methyl methacrylate) positive resist to pattern the first mask for metal contacts. Then a 25-nm thick layer of nickel is evaporated onto the device and a lift-off process leads to the definition of nickel contact regions. Nickel silicidation follows for the acquisition of NiSi contact pads for electrical characterization. Nickel silicidation is obtained by annealing performed by successive exposition of 20 min in forming gas at 200, 300, and 400 °C, respectively. Subsequently, a layer of 50 nm hydrogen silselsquioxane (HSQ), negative tone resist for electron beam lithography, is spin coated on top of the wafer and patterned into lines using electron beam lithography process followed by repeated Deep reactive ion etching cycles leading to vertically stacked, silicon nanowire structures anchored between two NiSi pillars.

2.2 Bio-functionalization Methodology

2.2.1 Memristive Biosensors

The fabricated memristive silicon nanowire structures are initially soaked in Piranha solution (mixture of sulfuric acid (H_2SO_4) and hydrogen peroxide (H_2O_2) in a ratio 3:1) for 30 min followed by rinsing with a copious amount of MilliQ water to remove any residual acid traces and drying with N_2 flow. Piranha solution cleans the sample surfaces from any organic residues and results in the activation of the silicon surface by generating more surface hydroxyl (−OH)-terminating groups and making it highly hydrophilic. Hydroxyl groups are serving as surface treatment for biomolecule grafting. Subsequently, different substrates of silicon nanowire arrays are functionalized by exposure to antibody solution with overnight incubation. For this, the nanostructures are separately incubated overnight at room temperature in dark in 1 mL solution of 250 μg/mL polyclonal rabbit anti-human PSA (Dako, A0562) in PBS (phosphate buffer saline; pH 7.2) filtered. After the incubation, all the substrates are gently washed three times with 1.5 mL of PBS-Tween 0.05 % solution and one final time with 1.5 mL of MilliQ water and then are left for 50 s to dry in air semicovered at room temperature. Afterwards, the substrates are separately incubated for 2 h in a 2-mL solution of PBS+BSA 1 % (bovine serum albumin) aiming at the prevention of the non-specific binding for the upcoming antigen uptake. In order to allow PBS+BSA 1 % to

be spread to all the regions of the substrate, during the incubation time, the substrates are placed on Heidolph Polymax 1040 Wave Motion Platform Shaker at 10 rpm speed at room temperature and fully covered with aluminum foil to prevent any exposure of the reagents to light. Then the structures are gently washed three times with 1.5 mL of PBS Tween 0.05 % and two times with 1.5 mL of MilliQ water and left for 50 s to dry before the antigen uptake.

2.3 Antigen Uptake

2.3.1 Detection

The functionalized structures are exposed to 880 μL of PSA-IgM (47 AU/mL) (Xeptagen Spa) solution within 1 h and 30 min incubation at room temperature in dark. Three diverse concentrations of biomarker are used separately at substrates originating from the same fabrication process, and the very same SOI wafer, with respect to the absolute biomarker concentration as shown in Table 1. In parallel, a substrate intended for fluorescence/confocal microscope study is equally incubated in a solution of 100 % concentration. The excess of antigen is removed by gently washing the substrates three times with 1.5 mL of PBS-Tween 0.05 % followed by one wash with 1.5 mL of MilliQ water. Then the substrates are left for 50 s drying at room temperature, semicovered in air.

2.4 SEM Imaging

Morphological analysis of the nanofabricated structures is carried out using Scanning Electron Microscopes MERLIN and Gemini500 from Zeiss, directly after the nanofabrication process and also after bio-modification of the surface. A 2-nm layer of iridium (Ir) is sputtered onto the bio-functionalized devices in order to avoid the protein charging effect and to provide the needed contrast to images.

2.5 Fluorescent Imaging

To verify the efficiency of the direct absorption methodology when dealing with the nanowire structures under study, substrate originating from the same fabrication process and the same SOI wafer is separately incubated overnight in 1 mL of 50 μg/mL α-mouse IgG-FITC from Sigma (F9006). After the incubation, the substrate is gently washed twice with 1.5 mL of PBS and once with MilliQ water and dried with N_2 flow. The confocal and transmission imaging microscope Yokogawa SPINNING-DISK CSU-W1 is used to obtain 3D signal distribution of the biomolecules.

Table 1 Concentrations of PSA-IgM biomarker

Concentration of PSA-IgM (AU/mL)	Percentage
47	100
23.5	50
11.75	25

2.6 Enzyme-Linked Immunosorbent Assay Study

The substrates are separately incubated for 1 h and 30 min in 2 ml of a-IgM-HRP secondary antibody, 1:1000 in XG-DB5 (dilution buffer, Xeptagen) solution, and afterwards, they are thoroughly washed five times with 1.5 mL of PBS-Tween 0.05 %. The substrates are separately transferred to new clean petri-plate holders and are anew extensively and intensively washed five times with 1.5 mL of PBS-Tween 0.05 % with 10–15-s incubation for each wash. Eventually, the structures are fully covered with 1 mL 2,2'-azino-bis(3-ethylbenzothiazoline-6-sulfonic acid (ABTS) in the dark at room temperature and ELISA tests follow. A solution of 100 μL is collected directly from the structure area after 10, 20, 30, and 40 min and placed in the ELISA wells. In parallel, negative control sample of 100 μL pure ABTS is also collected in ELISA wells of the same strip series to verify the measurements. Two consecutive ELISA measurements are performed with 20-min time difference.

3 Results and Discussion

3.1 Morphological Analysis

A nanofabricated device of initial mean width of 90 nm and 980 nm of length is presented in Fig. 1 after the fabrication process and surface treatment with piranha solution, before any bio-modification (above) and after bio-modification for

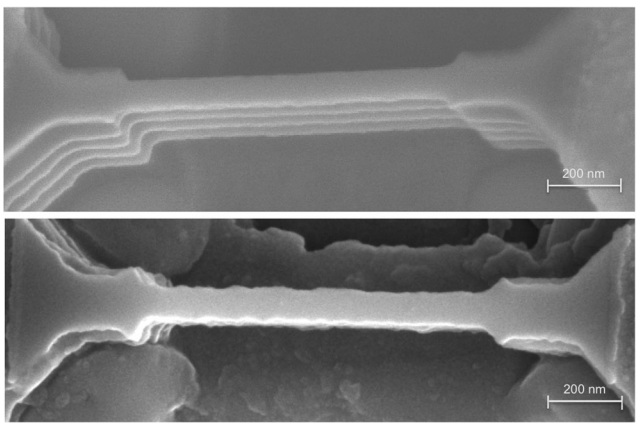

Fig. 1 Morphological scanning electron microscopic images acquired from the nanofabricated structure—Memristive device of initial mean width 90 nm and 980 nm of length and after the fabrication and surface treatment with piranha solution (above) after the final bio-modification with antigen of concentration 11.75 AU/mL (*bottom*)

the case of biomarker of a 11.75 AU/mL concentration (bottom).

Due to deep reactive ion etching process, the width along the structures is not perfectly homogenous. However, this is an advantage for our detection aim. In fact, the surface roughness finally enhances the binding of the proteins on the device by increasing the potential binding area and overall enables the bio-functionalization process. Figure 2 depicts a detail of the surface of nanofabricated structures after the bio-modification with 47 AU/mL concentration, where the biological substances are clearly shown. As it is indicated by repeating observation of SEM images taken from different devices of initial mean width 90 nm and 980 nm of length and for devices of initial mean width 38 nm and 410 nm of length, an increase in the device diameter is demonstrated due to the presence of the adsorbed layer of biomolecules on the nanowire surface. Accumulated data considering several measures along the structure on different devices depict a mean increase of the device diameter of 15.7 nm±2.7 nm. In some cases, agglomeration of protein molecules is present on the device surface as well as at the longitudinal sides of the device. According to RCSB PDB Protein Data Bank, the crystal structure of human prostate-specific antigen in a sandwich antibody complex is of dimension (5.53, 22.68, and 11.86 nm) defined by X-ray diffraction.

3.2 CLSM Measurements

The 3D fluorescence signal resulting from the confocal study is demonstrated in Fig. 3, where the fluorescence emitted by the antibody-coated layer deposited onto the bio-modified nanowire is clearly shown. This result is a further confirmation of the presence of the proteins onto the sensor, and it is in agreement with the diversion of the following electrical characteristics study.

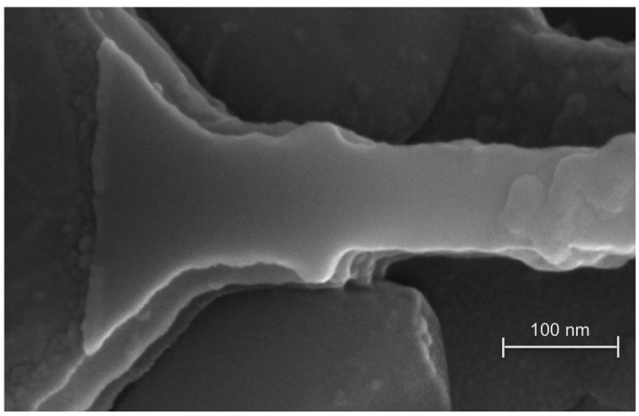

Fig. 2 Morphological scanning electron microscopic image acquired from the nanofabricated structure after the final bio-modification with antigen of concentration 47 AU/mL; detail of the device surface

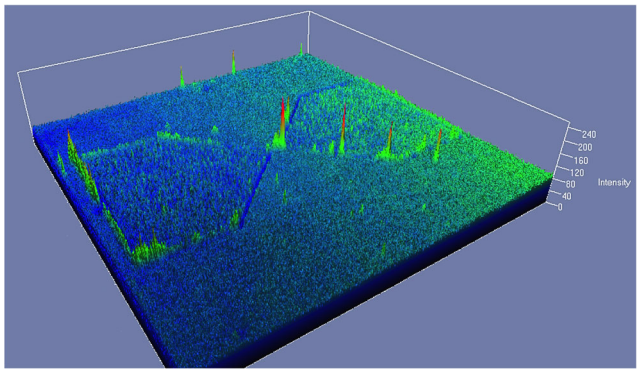

Fig. 3 3D fluorescent signal distribution plot acquired from the nanofabricated structure after the bio-modification of Si-NW

3.3 Electrical Measurements

The electrical characteristics of the memristive biosensors are obtained by measuring the current-to-voltage characteristics of the device structures of initial mean width 38 nm and 410 nm of length in air on dried samples using a Cascade Microtech Probe Station and a Hewlett-Packard 4165A Precision Semiconductor Parameter Analyzer.

The measurements are carried out at room temperature in air under a controlled humid environment of 20 % (rH%) [26]. For sensing measurement, a drain to source voltage sweep is performed forward and backward in the range from −2.4 to + 2.4 V. The back-gate potential VBG is kept grounded during the acquisition. A reference measurement is first applied on the fabricated structures just after the nanofabrication process and then followed by the electrical monitoring of memristive biosensors with antigen uptake. For bare nanofabricated wires, the semilogarithmic current-to-voltage characteristics indicate hysteretic loop at zero voltage as is it shown in Fig. 4. In these devices, the memory effect is due to the nanoscale dimensions of the device and it is strongly affected by charged molecules found in proximity of the surface. The hysteresis of the semilogarithmic curve acquired from bare device appears shifted from zero voltage to different voltage values associated with the net charge contribution of the biomolecules on the device surface. Namely, a voltage gap is created in the semilogarithmic current-to-voltage characteristics after the nanowire bio-modification as a further memory effect on the voltage scan across the memristive biosensor as also presented in Fig. 4 and reported in [20].

In the case studied, the conductance is strongly dependent on the charged species bound to the channel surface when a potential is applied to the device. Since each protein carries on charged residues, those charged residues of the biological substances act by creating an electrical field that affects the electrical characteristics of the device.

It is worth mentioning that the voltage gap exhibits a well repeatable behavior for the devices under study. Both probe antibodies and target antigens affect the memristive behavior.

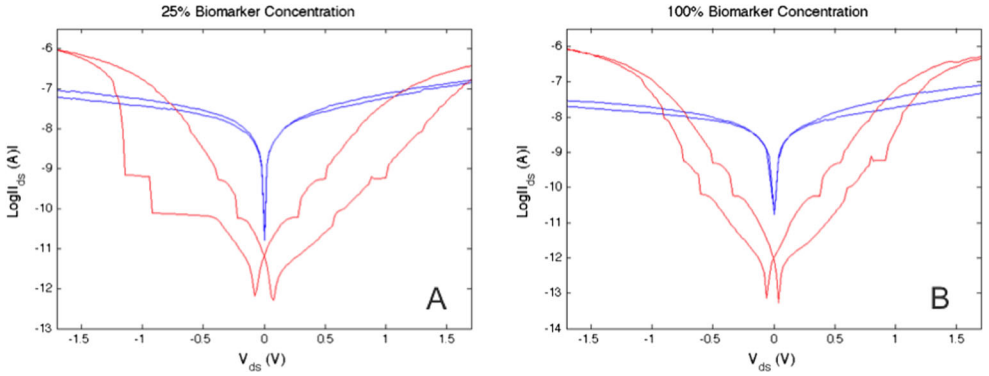

Fig. 4 Semilogarithmic current-to-voltage characteristics exhibited by a memristive-biosensor. Electrical characteristics for bare silicon nanowire-reference measurement-(*blue*) and for the same nanowire after the bio-modification of the surface for two different biomarker concentrations, minimum biomarker concentration (25 %) (**a**), and maximum biomarker concentration (100 %) (**b**) demonstrating voltage gaps of 0.16 and 0.1 V, respectively

After the bio-functionalization with antibodies, the voltage gap appears in the semilogarithmic current-to-voltage characteristics. The presence of antigens on the device surface seems to demonstrate the opposite effects comparing to those resulting due to the presence of the antibodies. Antigens are considered to have a masking contribution to the presence of antibodies. According to the previous arguments, the presence of antigens affects the width of the voltage gap which is already created by the presence of antibodies bringing a construction of the voltage difference. For the three different biomarker concentrations considered in the present study, the contraction of the voltage gap is depicted with increasing the biomarker concentration. Figure 4 shows the semilogarithmic current-to-voltage characteristics for identical devices treated with different concentrations of biomarkers. Collectively, the experimental data depict a slight but significant decrease of the hysteresis window, with respect to the values reported, when increasing the concentration of antigens, as it is demonstrated in Fig. 5 showing the average values obtained by 20 devices for each concentration. The error bars presented in Fig. 5 stand for the standard deviation of the sample studied. This error is largely dependent on the top-down fabrication process, which cannot result in perfectly homogenous structures.

3.4 ELISA Methodology

As expected, optical density in ELISA tests is increasing with time as a result of the progressively increasing ABTS reaction.

The diversity corresponding to the different biomarker concentrations is clearly shown. The optical density values as a function of time present different increasing trends for the different biomarker concentrations with the highest values of absorbance demonstrated by the highest concentration sample and the lowest values for the lowest concentration, respectively. Meanwhile, the negative control sample depicts constant values of optical density with respect to time for all the different concentration samples. These results indicate the importance of the detailed environmental control and of the intensive and thorough washing of the substrate between the different steps of the process. The fact that successful ELISA results are obtained from samples that had been subjected to consecutive intensive washes is a proof of the successful

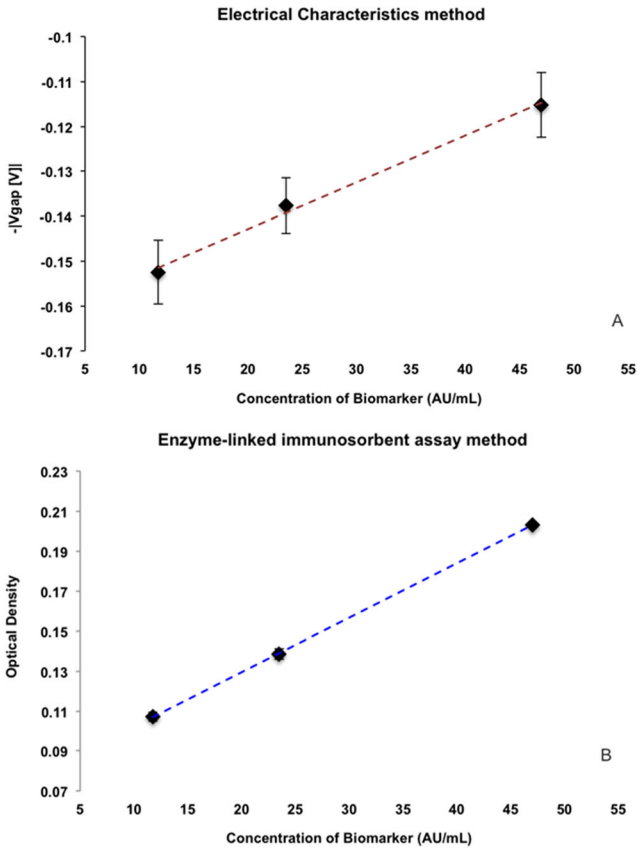

Fig. 5 Calibration curves obtained with electrical characteristic methodology for three diverse concentrations of biomarker uptaken on the surface (**a**) and with ELISA methodology for three diverse concentrations of biomarker uptaken on the surface over time obtained for two consecutive ELISA measurements performed with 20 min time difference (**b**)

binding of the biomolecules on the structures and moreover a further evidence of the sensitivity of the sensor in detection of even small quantities of biomarkers. Furthermore, the average values obtained for the different biomarker concentrations studied over time for the two consecutive ELISA measurements for the first 30 min of the experiments as shown in Fig. 5 indicate an increasing trend dependence of the optical density with the corresponding concentration of biomarker.

4 Conclusions

In the present study, memristive biosensors are fabricated and bio-functionalized with polyclonal rabbit anti-human PSA Ab to obtain biosensor devices that exhibit memristive electrical characteristics targeting at the sensing of PSA-IgM. Electrical measurements are implemented for the devices following the fabrication process and the final bio-modification of the devices with prostate cancer markers. The voltage gap appearing in the semilogarithmic current-to-voltage characteristics after the bio-modification of the devices demonstrates a well repeatable behavior and leads to a bio-detection method of PSA-IgM. Three different biomarker concentrations are studied, and a contraction of the voltage gap is depicted with increasing biomarker concentration. An equivalent dependence of the biomarker concentration is also observed in optical density measurements through the implementation of ELISA methodology. The optical density values present different increasing trends for diverse biomarker concentrations as a function of time as well as a function of the biomarker concentration. The correlation of the linear dependence trend presented with two different methodologies (electrical characterization and ELISA methodology) validates and verifies the efficiency of the memristive biosensors in sensing PSA-IgM in ranges useful for medical diagnosis.

Acknowledgments The authors gratefully acknowledge the staff of the Cmi Clean Room of EPFL for assisting with technical advice and M. Zervas for the fruitful discussions regarding the fabrication process and G. Knott for the SEM imaging with ZEISS Gemini500.

References

1. Lacroix-Desmazes, S., Kaveri, S. V., Mouthon, L., Ayouba, A., Malanchere, E., Coutinho, A., et al. (1998). Self-reactive antibodies (natural autoantibodies) in healthy individuals. *Journal of Immunological Methods, 216*, 117–137.
2. Varambally, S., Bar-Dayan, Y., Bayry, J., Lacroix-Desmazes, S., Horn, M., Sorel, M., et al. (2004). Natural human polyreactive IgM induce apoptosis of lymphoid cell lines and human peripheral blood mononuclear cells. *International Immunology, 16*, 517–524.
3. Pontisso, P., Calabrese, F., Benvegnu, L., Lise, M., Belluco, C., Ruvoletto, M. G., et al. (2004). Overexpression of squamous cell carcinoma antigen variants in hepatocellular carcinoma. *British Journal of Cancer, 90*, 833–837.
4. Beneduce, L., Castaldi, F., Marino, M., Tono, N., Gatta, A., Pontisso, P., et al. (2004). Improvement of liver cancer detection with simultaneous assessment of circulating levels of free alpha-fetoprotein (AFP) and AFP-IgM complexes. *The International Journal of Biological Markers, 19*, 155–159.
5. Beneduce, L., Castaldi, F., Marino, M., Quarta, S., Ruvoletto, M., Benvegnu, L., et al. (2005). Squamous cell carcinoma antigen IgM complexes as novel biomarkers for hepatocellular carcinoma. *Cancer, 103*, 2558–2565.
6. Pontisso, P., Quarta, S., Caberlotto, C., Beneduce, L., Marino, M., Bernardinello, E., et al. (2006). Progressive increase of SCCAIgM immune complexes in cirrhotic patients is associated with development of hepatocellular carcinoma. *International Journal of Cancer, 119*, 735–740.
7. Castaldi, F., Marino, M., Beneduce, L., Belluco, C., De Marchi, F., Mammano, E., et al. (2005). Detection of circulating CEAIgM complexes in early stage (stage 1) colorectal cancer. *The International Journal of Biological Markers, 20*, 204–208.
8. Goc, S., & Jankovic, M. (2013). Evaluation of molecular species of prostate-specific antigen complexed with immunoglobulin M in prostate cancer and benign prostatic hyperplasia. *Disease Markers, 35*(6), 847–855.
9. Beneduce, L., Prayer-Galetti, T., Giustinian, A. M., Gallotta, A., Betto, G., Pagano, F., et al. (2007). Detection of prostate-specific antigen coupled to immunoglobulin M in prostate cancer patients. *Cancer Detection and Prevention, 31*(5), 402–7.
10. Strukov, D., Snider, G., Stewart, D., Williams, S. (2008). The missing memristor found. *Nature, 453*, 80–83.
11. Chua, L. (1971). Memristor—the missing circuit element. *IEEE Transactions on Circuit Theory, 18*(5), 507–519.
12. Wua, J., & Mc Creery, R. (2009). Solid-state electrochemistry in molecule/TiO2 molecular heterojunctions as the basis of the TiO2 memristor. *Journal of the Electrochemical Society, 156*(1), 29–37.
13. Rose, G., Rajendran, J., Manem, H., Karri, R., Pino, R. (2012). Leveraging memristive systems in the construction of digital logic circuits. *Proceedings of the IEEE, 100*(6), 2033–2049.
14. Pershin, Y., & Di Ventra, M. (2010). Experimental demonstration of associative memory with memristive neural networks. *Neural Networks, 23*(7), 881–886.
15. Indiveri, G., Linares-Barranco, B., Legenstein, R., Deligeorgis, G., Prodromakis, T. (2013). Integration of nanoscale memristor synapses in neuromorphic computing architectures. *Nanotechnology, 24*, 384010.
16. Gelencser, A., Prodromakis, T., Toumazou, C., Roska, T. (2012). Biomimetic model of the outer plexiform layer by incorporating memristive devices. *Physical Review E, 85*, 041918.
17. Sacchetto, D., Gaillardon, P. E., Zervas, M., Carrara, S., De Micheli, G., Leblebici, Y. (2013). Applications of multi-terminal memristive devices: a review. *IEEE Circuits and Systems, 13*(2), 23–41.
18. Gaillardon, P. E., Sacchetto, D., Bobba, S., Leblebici, Y. (2012). *GMS: generic memristive structure for non-volatile FPGAs*. Santa Cruz: IFIP/IEEE International Conference on Very Large Scale Integration (VLSI-SoC).
19. Sacchetto, D., Doucey, M. A., De Micheli, G., Leblebici, Y., Carrara, S. (2011). New insight on biosensing by nano-fabricated memristors. *BioNanoScience, 1*, 1–3.
20. Carrara, S., Sacchetto, D., Doucey, M. A., Baj-Rossi, C., De Micheli, G., Leblebici, Y. (2012). Applications of multi-terminal memristive devices: a review. *Sensors Actuators B: Chemical, 171–172*, 449–457.
21. Patolsky, F., Zheng, G., Lieber, C. M. (2006). Fabrication of silicon nanowire devices for ultrasensitive, label-free, real-time detection of biological and chemical species. *Nature Protocols, 1*, 1711–1724.

22. Zhou, X. T., Hu, J. Q., Li, C. P., Ma, D. D. D., Lee, S. T. (2003). Silicon nanowires as chemical sensors. *Chemical Physics Letters, 369*, 220–224.
23. Janata, J., & Josowicz, M. (2003). Conducting polymers in electronic chemical sensors. *Nature Materials, 2*, 19–24.
24. Zheng, G., Patolsky, F., Cuil, Y., Wang, W., Lieber, C. (2005). Multiplexed electrical detection of cancer markers with nanowire sensor arrays. *Nature Biotechnology, 23*(3), 12941301.
25. Stern, E., Vacic, A., Mark, A. R. (2008). Semiconducting nanowire field effect transistor biomolecular sensors IEEE trans. *Electronic Devices, 55*(11), 31193130.
26. Puppo, F., Dave, A., Doucey, M. A., Sacchetto, D., Baj-Rossi, C., Leblebici, Y., et al. (2014). Memristive biosensors under varying humidity conditions. *IEEE Transactions on NanoBioscience, 13*(1), 19–30.